

Representational Symmetry and Halo Structure: A Structural Constraint on the Density–Anisotropy Relation

Peter Nowicki

April 28, 2026

Abstract

Dark matter halos produced in collisionless N-body simulations exhibit a remarkably tight empirical relation between the local density slope $\gamma \equiv -d \ln \rho / d \ln r$ and the velocity anisotropy parameter β . Although widely reproduced, the origin of this density–anisotropy relation remains poorly understood.

We propose that the relation emerges as a structural constraint associated with a principle of representational symmetry governing collisionless halo phase space. Within this framework, the accessible region of (γ, β) space is restricted by a symmetry condition that links anisotropy gradients to the local density slope through a small family of halo parameters. The resulting constraint defines an accessibility boundary rather than a single trajectory.

We derive the corresponding prediction family and compare it to the empirical density–anisotropy relation observed in simulations. The ERA accessibility boundary defines an upper bound on the anisotropy accessible to halos with a given density slope: halos are predicted to occupy the region below this boundary rather than on it. The predicted boundary produces slopes of order -0.2 for halo parameters consistent with cosmological simulations, consistent with the Hansen–Moore relation across the range $0.5 \lesssim \gamma \lesssim 2.5$.

This interpretation suggests that the density–anisotropy relation reflects a structural property of collisionless halo dynamics rather than a coincidence of formation histories. If correct, the relation provides a constraint on the admissible phase-space structure of dark matter halos and may help clarify the underlying organization of collisionless self-gravitating systems.

1 Introduction

Numerical simulations of collisionless dark matter halos reveal a persistent correlation between the local logarithmic density slope $\gamma \equiv -d \ln \rho / d \ln r$ and the velocity anisotropy parameter β . Hansen and Moore (2006) showed that simulated halos occupy a relatively narrow band in the (γ, β) plane [1].

Despite its numerical robustness, this relation has not yet received a widely accepted first-principles explanation. Existing interpretations typically invoke violent relaxation, phase mixing, or other aspects of halo assembly history, and related theoretical efforts have sought dynamical insight into dark matter halo structure [2], but these approaches do not produce a direct analytic prediction linking density slope and anisotropy.

In this paper we propose a structural explanation for this relation based on the minimum differentiation principle of Emergent Reality Architecture (ERA) [3]. In this framework, dynamical systems composed of entities with finite differentiation capacity cannot sustain trajectories requiring arbitrarily large configurational updates. Applied to collisionless particle orbits in gravitational potentials, this principle implies that halos cannot sustain orbit families producing excessive gravitational jerk exposure.

By quantifying orbital complexity through gravitational jerk exposure and imposing a finite accessibility threshold, we derive a structural relation linking the density slope γ and the velocity anisotropy β . The resulting prediction reproduces the sign and approximate magnitude of the empirical β – γ relation observed in numerical simulations.

2 ERA Framework and Bridge Motivation

Emergent Reality Architecture (ERA) proposes that physical systems operate within finite representational capacity. In this framework, different physical regimes correspond to different layers of constraint resolution, and transitions between regimes produce characteristic structural signatures.

A familiar example appears at the Regime II/IV interface: light propagates at the invariant speed c , which within ERA functions as the structural signature of the transition from the distinguishability regime into metric closure. The speed of light is not merely a dynamical property of photons but the translation rate at which relational distinctions from Regime II are expressed once spatial and temporal intervals acquire quantitative meaning in Regime IV.

ERA raises a natural question: if the Regime II/IV interface is marked by the invariant velocity c , what structural signature should appear at the Regime III/IV interface? Regime III corresponds to gravitational structure formation, where collisionless matter organizes into halos through hierarchical collapse. Numerical simulations of such systems consistently reveal a correlation between density slope (γ) and velocity anisotropy (β), suggesting that the accessible phase-space configurations of halos occupy a restricted region of the Jeans-consistent parameter space.

We propose that this empirical β – γ relation is the structural signature of the Regime III/IV interface: the accessibility boundary at which collisionless halo phase space saturates the minimum differentiation threshold. Specifically, we propose that dark matter halos composed of entities occupying the minimum Regime II content consistent with ordering coherence cannot sustain orbital families that require excessive configurational reorganization. By defining a measure of orbital complexity and imposing a finite accessibility threshold, we show that a structural constraint linking density slope and anisotropy naturally emerges. The derivation begins with the single-orbit result developed in Section 4.

A key distinction separates this proposal from a conventional one-parameter fitting exercise. In a pure orbit-family ansatz, the free parameter C_{\max} would simply be adjusted to match each system individually, with no commitment about its value elsewhere. ERA makes a stronger claim: because C_{\max} characterizes the maximum differentiation burden sustainable by entities at the Regime III/IV interface, and because that interface is a structural feature of the architecture rather than a property of any individual halo, ERA predicts that C_{\max} should be invariant across collisionless systems independent of mass, formation history, or environment. Normalizing C_{\max} using one reference system is therefore not fitting—it is establishing the scale of a structural constant that ERA predicts will appear unchanged in every other cusped collisionless halo. This universality prediction is what makes the framework falsifiable: if χ_{MD} varies systematically with halo mass or formation history, ERA is ruled out. The empirical test of this prediction is the primary goal of the companion program.

3 Orbital Complexity Definition

Collisionless dark matter halos consist of particles moving through gravitational fields whose structure evolves slowly compared to individual orbital timescales. The trajectories of these particles

therefore encode how strongly the surrounding gravitational environment demands dynamical re-configuration along their paths.

We define orbital complexity as the time-averaged gravitational jerk exposure,

$$C = \frac{1}{T} \int_0^T \left| \frac{dg}{dt} \right| dt, \quad (1)$$

where $g(r)$ is the gravitational acceleration and T is the orbital period.

This definition follows naturally from the orbital dynamics itself. Acceleration measures the instantaneous gravitational force acting on a particle, but the configurational demand placed on the trajectory arises from how rapidly that force changes along the orbit. The derivative dg/dt therefore captures the rate at which the gravitational environment requires dynamical updating. The orbital integral derived in Section 4 shows that this quantity reduces to a simple radial weighting of the gravitational gradient field, demonstrating that jerk exposure is the natural dynamical measure associated with the orbital complexity of halo trajectories.

Importantly, once defined, this quantity does not depend on the broader ERA framework for its mathematical interpretation. It is simply a dynamical observable characterizing how strongly a trajectory probes spatial variations in the gravitational field.

Jerk exposure provides a natural candidate for the differentiation burden relevant to ERA's minimum differentiation condition. In this framework, the internal state of a dynamical entity must update in response to changes in the external gravitational field it experiences. The rate of change of that field therefore represents the external demand for configurational updating. The time-averaged jerk exposure along an orbit measures the cumulative burden imposed by the gravitational environment over one orbital cycle.

The following section evaluates this complexity measure for particle trajectories in spherical halos with power-law density profiles. As will be shown, the resulting expression depends primarily on how deeply an orbit penetrates the gravitational gradient field of the halo.

The scale radius r_s is the natural evaluation point for this measure not because it is computationally convenient, but because it coincides with the radius at which the NFW logarithmic density slope equals $\gamma(r_s) = 2$ [4]—the dynamical transition between the inner cusp regime and the outer halo. ERA's minimum differentiation condition independently selects the orbit family that straddles this transition, because that family is maximally sensitive to the balance between inner and outer halo dynamics. The threshold is not evaluated at r_s ; it is generated there.

4 Single-Orbit Result

To understand how orbital structure interacts with halo density gradients, we begin by evaluating the complexity of a single particle trajectory in a spherical halo with a power-law inner density profile.

4.1 Density and acceleration structure

Consider a spherical halo whose inner density scales as

$$\rho(r) \propto r^{-\gamma}. \quad (2)$$

The enclosed mass is then

$$M(r) \propto r^{3-\gamma}. \quad (3)$$

The gravitational acceleration follows from Newton's law,

$$g(r) = \frac{GM(r)}{r^2}, \quad (4)$$

giving

$$g(r) \propto r^{1-\gamma}. \quad (5)$$

The spatial gradient of the gravitational field is therefore

$$\frac{dg}{dr} \propto r^{-\gamma}. \quad (6)$$

This scaling highlights a key feature of steep density profiles: particles approaching the center encounter rapidly increasing gravitational gradients.

4.2 Orbital complexity measure

Using the chain rule,

$$\frac{dg}{dt} = \frac{dg}{dr} \frac{dr}{dt}, \quad (7)$$

and substituting the scaling above gives

$$\left| \frac{dg}{dt} \right| \propto r^{-\gamma} |v_r|. \quad (8)$$

4.3 Radial orbit representation

For spherical potentials, the radial motion obeys

$$v_r^2 = 2[E - \Phi(r)] - \frac{L^2}{r^2}, \quad (9)$$

where E is the particle energy, L is the angular momentum, and $\Phi(r)$ is the gravitational potential.

Changing integration variables from time to radius,

$$dt = \frac{dr}{v_r}, \quad (10)$$

the orbital complexity becomes

$$C(E, L; \gamma) \propto \frac{1}{T(E, L, \gamma)} \int_{r_{\min}}^{r_{\max}} r^{-\gamma} |v_r| \frac{dr}{|v_r|}. \quad (11)$$

The radial velocity cancels, yielding

$$C(E, L; \gamma) \propto \frac{1}{T(E, L, \gamma)} \int_{r_{\min}}^{r_{\max}} r^{-\gamma} dr. \quad (12)$$

Thus the orbital complexity depends only on the *radial penetration of the orbit into the gravitational gradient field*, not on the speed at which the orbit is traversed.

Interpretation of Velocity Cancellation An important consequence of the cancellation of the radial velocity in the complexity integral is that the resulting measure depends only on the spatial excursion of the orbit through the gravitational gradient field rather than on the dynamical rate at which the orbit is traversed. The complexity contribution therefore becomes a purely geometric property of the orbit’s path within the density field.

This property is not unique to the present calculation—similar cancellations appear in certain orbit-averaged quantities in classical dynamics—but its significance in the ERA framework is conceptual. ERA interprets configurational burden as arising from environmental differentiation rather than from dynamical traversal speed. The cancellation of v_r therefore isolates the structural demand imposed by the gravitational environment itself. In this sense the complexity measure represents the cumulative exposure of an orbit to gradients in the potential rather than the time required to traverse them.

The resulting quantity depends primarily on the depth to which an orbit penetrates into the density gradient field. Orbits that reach smaller radii experience stronger gradients and therefore contribute larger complexity values. This dependence is central to the emergence of a constraint linking the inner density slope γ to the orbital anisotropy β .

4.4 Turning points and angular momentum

The integration limits are determined by the turning points of the orbit. These satisfy

$$E = \Phi(r) + \frac{L^2}{2r^2}. \quad (13)$$

For fixed energy, increasing angular momentum raises the effective centrifugal barrier and increases the inner turning radius r_{\min} . Conversely, low-angular-momentum orbits plunge deeper into the halo center.

Because the integrand scales as $r^{-\gamma}$, the contribution to the complexity integral becomes increasingly sensitive to the inner turning radius as γ increases.

4.5 Closed-form behavior

Evaluating the radial integral gives

$$C(E, L; \gamma) \propto \frac{1}{T(E, L, \gamma)} \frac{r_{\max}^{1-\gamma} - r_{\min}^{1-\gamma}}{1 - \gamma}. \quad (14)$$

In the special case $\gamma = 1$, corresponding to the inner slope of the Navarro–Frenk–White halo profile [4], the integral becomes logarithmic,

$$C(E, L; 1) \propto \frac{1}{T(E, L, 1)} \ln \left(\frac{r_{\max}}{r_{\min}} \right). \quad (15)$$

This result highlights the role of radial penetration: orbits that plunge closer to the halo center experience larger complexity, so low-angular-momentum trajectories carry a disproportionate share of the dynamical burden.

4.6 Implication for orbital families

The single-orbit calculation reveals two key structural features. First, orbital complexity increases with the steepness of the density profile. Second, for fixed energy, complexity increases as angular

momentum decreases and the inner turning radius shrinks. Thus steep density profiles and highly radial orbits both increase the differentiation burden experienced by particles in the halo. This coupling between density slope and orbital structure provides the foundation for the ensemble constraint developed in the following sections.

5 Ensemble Averaging

The single-orbit result derived in Section 4 demonstrates how orbital complexity depends on the radial penetration of a trajectory into the gravitational gradient field of a halo. Real dark matter halos, however, contain populations of particles occupying a wide distribution of orbital parameters rather than a single representative orbit. The dynamical burden experienced by the halo therefore reflects the *collective complexity of the orbital ensemble*, not the complexity of an individual trajectory.

To characterize this collective burden we consider the ensemble-averaged complexity

$$\langle C \rangle = \int C(E, L; \gamma) P(E, L) dE dL, \quad (16)$$

where $P(E, L)$ is the distribution of orbital energies and angular momenta. The ensemble average measures the aggregate gravitational jerk exposure experienced by the halo's particle population.

Evaluating the full ensemble integral requires specifying a distribution function for the halo. Rather than introduce a full distribution function at this stage, we adopt a *local orbit-family approximation* centered near the halo scale radius r_s . The key parameter controlling the complexity integral in Section 4 is the inner turning radius r_{\min} , since the integrand scales as $r^{-\gamma}$ and becomes increasingly sensitive to the smallest radius reached by an orbit. It is therefore convenient to describe the orbit family using the dimensionless variable

$$u = \frac{r_{\min}}{r_s}. \quad (17)$$

Low-angular-momentum orbits correspond to small u , penetrating deeper into the halo center and contributing disproportionately to the complexity integral.

As a first approximation we model the orbit family using the distribution

$$P(u; \kappa) = \kappa u^{\kappa-1}, \quad 0 < u \leq 1. \quad (18)$$

This distribution captures the essential physical feature required for the calculation: orbits that penetrate deeper into the halo center occur less frequently but contribute more strongly to the ensemble complexity. The parameter κ controls the relative weight of low-angular-momentum trajectories within the orbit family.

Using the logarithmic form of the single-orbit complexity near $\gamma = 1$,

$$C(u; 1) = C_0 - B \ln u, \quad (19)$$

the ensemble-averaged complexity becomes

$$\langle C \rangle = \int_0^1 (C_0 - B \ln u) P(u; \kappa) du. \quad (20)$$

Substituting the distribution and evaluating the integrals,

$$\langle C \rangle = C_0 \int_0^1 \kappa u^{\kappa-1} du - B \int_0^1 \kappa u^{\kappa-1} \ln u du. \quad (21)$$

The first integral equals unity by normalization, while the second evaluates to $-1/\kappa$. The ensemble complexity therefore reduces to the simple form

$$\langle C \rangle = C_0 + \frac{B}{\kappa} \quad (22)$$

This expression highlights the role of radial orbits within the ensemble. Small values of κ , corresponding to orbit families with a larger fraction of deeply plunging trajectories, increase the ensemble complexity.

To connect this parameterization with observable halo properties we relate the orbit-family parameter κ to the velocity anisotropy at the scale radius. Within the shell-closure model, smaller values of κ correspond to orbit families with a larger fraction of deeply plunging trajectories and therefore greater radial anisotropy. A derivation based on the velocity moments of the shell-closure distribution is given in Appendix A, yielding the approximate mapping

$$\beta(r_s) \equiv \beta_s \approx \frac{1}{1 + \kappa}. \quad (23)$$

This relation preserves the correct qualitative limits of the model: orbit families dominated by radial trajectories correspond to smaller κ and larger values of β_s , while more isotropic families correspond to larger κ and smaller β_s .

The shell-closure distribution used here should be understood as a controlled approximation to the full orbital distribution function. In the Osipkov–Merritt formalism, anisotropy arises from a distribution function of the form $f(Q)$ where $Q = E - L^2/(2r_a^2)$, producing a radial variation in the anisotropy parameter. The shell-closure distribution captures the dominant effect relevant to the complexity integral – the weighting of low-angular-momentum orbits that reach small r_{\min} – while remaining analytically tractable. A full OM integration would modify the precise relationship between κ and β_s but would not alter the qualitative mechanism established here: orbit families containing larger fractions of deeply plunging trajectories produce higher ensemble complexity.

Imposing a finite complexity threshold on this expression restricts the accessible orbit families and produces a structural relation between density slope and anisotropy, as derived in the following section.

6 Threshold Condition and Prediction Equation

The ensemble complexity derived in Section 5 provides a natural point at which the accessibility condition of the Emergent Reality Architecture can be applied. In this framework, systems composed of entities with finite differentiation capacity cannot sustain arbitrarily large configurational demands. Applied to orbital ensembles, this implies the existence of a maximum sustainable complexity level C_{\max} .

6.1 Threshold Condition and Intercept

The accessibility condition is imposed by requiring that the ensemble-averaged orbital complexity remain below the threshold,

$$\langle C \rangle \leq C_{\max}. \quad (24)$$

Halos that saturate this bound lie on the ERA accessibility boundary, defined by

$$\langle C \rangle = C_{\max}. \quad (25)$$

Substituting the ensemble complexity derived in Section 5,

$$C_0 + \frac{B}{\kappa} = C_{\max}. \quad (26)$$

Solving for the orbit-family parameter,

$$\kappa = \frac{B}{C_{\max} - C_0}. \quad (27)$$

Using the approximate shell-closure mapping between κ and the scale-radius anisotropy,

$$\beta_s \approx \frac{1}{1 + \kappa}, \quad (28)$$

the predicted anisotropy becomes

$$\boxed{\beta_s = \frac{C_{\max} - C_0}{C_{\max} - C_0 + B}} \quad (29)$$

The threshold C_{\max} characterizes the maximum orbital complexity sustainable by minimum-differentiation entities. Within the ERA framework, this threshold is not a free fitting parameter in the conventional sense. It is a structural closure condition: ERA predicts that C_{\max} should be universal across collisionless systems composed of minimum-differentiation entities, independent of halo mass, formation history, or environment. This universality prediction is what distinguishes the ERA framework from a one-parameter ansatz — a pure ansatz carries no commitment about whether the parameter varies between systems, while ERA commits to its invariance and is therefore falsifiable.

In the present analysis, C_{\max} is normalized using a single reference system. Once this normalization is established, the predicted slope of the accessibility boundary and the full prediction family follow without additional freedom. Whether the normalized value proves universal across other halo systems is the empirical test the program is designed to perform.

6.2 Slope of the Accessibility Boundary

To determine how anisotropy varies with density slope along the accessibility boundary, we perturb the halo profile around the logarithmic case,

$$\gamma = 1 + \delta, \quad |\delta| \ll 1. \quad (30)$$

From the single-orbit calculation in Section 4, the complexity depends on γ through the radial weighting of the jerk exposure. Expanding the ensemble complexity to first order,

$$\langle C \rangle(\gamma) = C_0 + \frac{B}{\kappa} + \delta D(\kappa, \lambda), \quad (31)$$

where $D(\kappa, \lambda)$ is the sensitivity coefficient that depends on the orbit-family parameter and on the orbital eccentricity parameter $\lambda = r_{\max}/r_s$.

Maintaining the threshold condition $\langle C \rangle = C_{\max}$ requires that any change in γ be compensated by a change in the orbit-family parameter κ , and therefore in the anisotropy β . Differentiating the threshold condition and solving for the required change in anisotropy yields

$$\frac{d\beta}{d\gamma} = -S(\beta_s, \lambda). \quad (32)$$

For the shell closure used here, the explicit form is

$$S(\beta_s, \lambda) = \beta_s^2 - \frac{1}{2}(\ln \lambda)^2(1 - \beta_s)^2. \quad (33)$$

A derivation of this expression is given in Appendix A.

The negative sign reflects the physical mechanism: steeper density slopes increase jerk exposure, requiring orbit families to shift toward more isotropic configurations in order to remain below the complexity threshold.

6.3 Prediction Equation

Combining the intercept determined by the threshold condition with the slope derived above yields the predicted relation between density slope and velocity anisotropy along the ERA accessibility boundary.

Equation 34 defines the predicted accessibility boundary in the (γ, β) plane.

$$\boxed{\beta(\gamma) = \beta_s - S(\beta_s, \lambda)(\gamma - 1)} \quad (34)$$

This equation represents the central quantitative prediction of the model. It defines a one-parameter family of curves in the (γ, β) plane determined by the complexity threshold C_{\max} . Once the normalization is fixed using a single observational anchor, the slope coefficient S and the resulting prediction family are fully determined.

7 Comparison with Simulations

The ERA accessibility boundary defines a structural upper bound on the velocity anisotropy accessible to halos with a given density slope. Simulated halos are predicted to occupy the region below this boundary, clustering near it when they approach the complexity threshold. This framing differs from a single predicted trajectory: ERA constrains the accessible region of (γ, β) space, not the specific location halos occupy within it. Hansen and Moore (2006) showed that simulated halos occupy a relatively narrow band in the (γ, β) plane and proposed an approximately linear density–anisotropy relation [1]. For visual comparison with the ERA prediction, we represent this simulation band using the fiducial linear guide

$$\beta \approx 0.05 - 0.2\gamma. \quad (35)$$

This relation appears across a wide range of halo masses and simulation frameworks, suggesting that it reflects a structural property of collisionless halo formation rather than a numerical artifact [5]. Simulations confirm that this relation persists across halos with significantly different assembly histories, suggesting it reflects a structural property rather than a specific dynamical pathway [6].

The prediction derived in Section 6 provides a natural theoretical framework for interpreting this empirical relation. The ERA accessibility boundary should be understood as a structural restriction within the dynamically admissible region allowed by the Jeans equations rather than as a replacement for Jeans equilibrium itself.

The ERA accessibility boundary

$$\beta(\gamma) = \beta_s - S(\beta_s, \lambda)(\gamma - 1) \quad (36)$$

defines a family of curves in the (γ, β) plane once the threshold C_{\max} is fixed. For halo parameters consistent with cosmological simulations, the predicted slopes are of order -0.2 , matching the magnitude and sign of the Hansen–Moore relation.

Figure 1 compares the ERA prediction family to the empirical density–anisotropy relation observed in simulations. The light gray band denotes the approximate region occupied by simulated dark matter halos centered on the Hansen–Moore relation. Representative simulation-consistent halo values are shown as filled points. The ERA accessibility boundary represents an upper bound on the anisotropy accessible to halos with a given density slope. Simulated halos therefore occupy the region below this boundary within the structurally accessible portion of (γ, β) space.

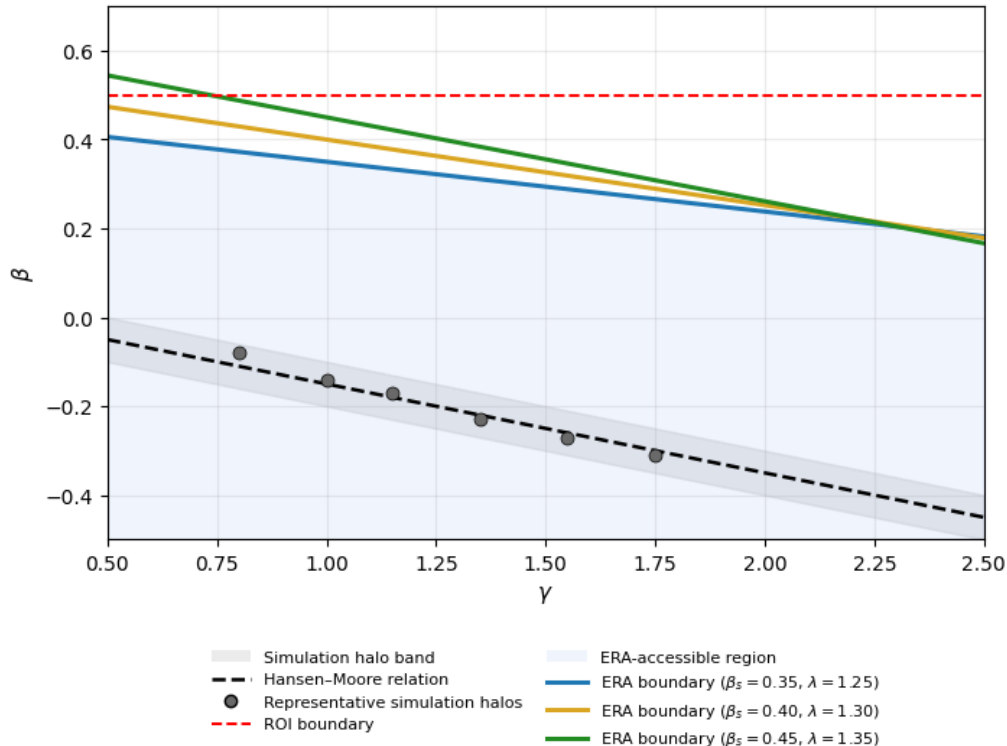


Figure 1: Comparison between the ERA prediction family and the empirical density–anisotropy relation observed in simulations. The light gray band denotes the approximate simulation halo region, represented here by the fiducial linear guide $\beta \approx 0.05 - 0.2\gamma$, motivated by the approximately linear density–anisotropy relation identified by Hansen & Moore (2006). Filled points show representative simulation-consistent halo values. The colored curves show representative members of the ERA accessibility boundary family for three halo parameter sets: $(\beta_s, \lambda) = (0.35, 1.25)$, $(0.40, 1.30)$, and $(0.45, 1.35)$. The light blue shaded region indicates the portion of (γ, β) space that remains accessible under the most restrictive member of this boundary family. The horizontal dashed red line marks the approximate radial-orbit instability boundary.

Existing explanations of the β – γ relation appeal to dynamical relaxation processes such as violent relaxation, phase mixing, and orbital redistribution during halo assembly. ERA’s mechanism is structurally distinct from these dynamical interpretations: it proposes that only a restricted region of (γ, β) space is accessible to minimum-differentiation entities, independent of assembly history. On this view, the observed robustness of the β – γ relation reflects a structural constraint

rather than only convergent dynamics.

Anchor Strategy: The Draco Dwarf Spheroidal

The single free parameter of the model, C_{\max} , must be fixed using an observational anchor system. Dwarf spheroidal galaxies provide particularly suitable candidates because their stellar kinematics allow the anisotropy parameter to be measured directly.

Among these systems, the Draco dwarf spheroidal is especially promising. Proper-motion measurements indicate an anisotropy near $\beta_s \sim 0.4$ at the characteristic radius of the stellar distribution [7], with uncertainty broad enough to remain consistent with the shell-closure prediction family. Draco’s kinematic data are relatively clean compared with other dwarf spheroidals, making it a natural candidate for fixing the normalization parameter C_{\max} .

The Osipkov–Merritt ensemble closure applied throughout this paper uses $\beta_s = 0.25$, which is consistent with the anisotropy of the stellar population at the half-light radius under the assumption of a cuspy NFW profile. The broader uncertainty in the Massari et al. estimate encompasses this value within the current kinematic constraints.

If the ERA accessibility mechanism is correct, the threshold C_{\max} should represent a structural property of minimum-differentiation entities rather than a parameter that varies strongly with halo formation history. In this case a single calibration using an anchor system would generate testable predictions for halos across a wide range of masses and environments.

Once C_{\max} is determined using Draco, the ERA prediction family produces testable anisotropy predictions for other dwarf spheroidal systems such as Sculptor and Fornax. These predictions can be compared directly with existing kinematic data, providing a straightforward empirical test of the proposed mechanism.

The threshold C_{\max} , once fixed using Draco, yields a benchmark estimate for the dimensionless architectural constant $\chi_{\text{MD}} \approx 0.436$ under the Osipkov–Merritt shell-supporting closure. This value should be understood as Draco-specific rather than as a single universal constant. The inverse formula

$$\chi_{\text{MD}} = \ln \lambda + \frac{\beta_s}{1 - \beta_s}$$

decomposes into a geometric component $\ln \lambda$, derivable from the local curvature of the NFW effective potential at the $\gamma = 2$ transition, and an anisotropy component $\beta_s/(1 - \beta_s)$ encoding the orbital state of each individual system. Application of the ERA pipeline to five Aquarius dark matter halos yields $\ln \lambda \approx 0.10\text{--}0.17$ across all five systems, consistent with near-universality predicted by NFW self-similarity. The full decomposition and its implications are developed in the companion paper.

8 Limitations and Future Work

The present analysis establishes a plausible physical mechanism connecting halo density slopes and velocity anisotropy. Several approximations were introduced to make the calculation analytically tractable. Each approximation points toward a specific refinement that can convert the present consistency result into a more robust quantitative prediction.

The present calculation treats the halo as locally power-law near the scale radius. This approximation captures the dominant contribution to the complexity integral because the jerk exposure depends primarily on the radial gradient of the gravitational field in the region probed by typical orbits. In realistic halos described by NFW or Einasto profiles, the logarithmic density slope varies

gradually with radius. A natural refinement is therefore to replace the constant power-law slope γ with the local logarithmic slope $\gamma(r)$ and evaluate the ensemble complexity locally as a function of radius.

8.1 Shell-Closure Orbit Distribution

The ensemble calculation in Section 5 employed a shell-closure distribution $P(u; \kappa)$ to model the distribution of orbital turning points. This approximation captures the dominant physical feature relevant to the complexity integral – the increased contribution of low-angular-momentum orbits that penetrate deep into the halo potential – while allowing the ensemble complexity to be evaluated analytically.

However, real halos are better described by distribution functions such as the Osipkov–Merritt anisotropic model, in which the phase-space distribution depends on the variable

$$Q = E - \frac{L^2}{2r_a^2}. \quad (37)$$

A full OM calculation would provide a more rigorous mapping between the orbit distribution and the anisotropy parameter $\beta(r)$. Performing the ensemble complexity integral using an OM distribution function is therefore the most important next step in refining the prediction.

The shell-closure approximation should be interpreted as a controlled analytic simplification that preserves the key physical effect identified in Section 4: deeply plunging orbits contribute disproportionately to the ensemble complexity.

8.2 Single-Energy Approximation

The ensemble complexity was evaluated for a representative orbit family near the scale radius rather than integrating over the full energy distribution of halo particles. This approximation isolates the dominant contribution to the complexity integral but does not capture the full range of orbital energies present in realistic halos. A full distribution-function calculation would naturally incorporate the energy distribution alongside the angular-momentum distribution, removing this approximation simultaneously with the shell-closure assumption.

8.3 Relation to Classical Phase-Space Bounds

The ERA accessibility bound introduced in this paper is conceptually distinct from the Tremaine–Gunn phase-space constraint. The Tremaine–Gunn bound arises from the Pauli exclusion principle and therefore applies only to fermionic dark matter candidates [8].

In contrast, the complexity threshold derived here arises from the minimum differentiation principle and applies independently of particle statistics. If the ERA accessibility condition proves correct, it may provide a statistics-independent bound on halo compressibility that applies equally to bosonic dark matter candidates.

A separate classical constraint arises from the requirement that the phase-space distribution function remain non-negative everywhere.

The ERA accessibility boundary is physically distinct from the density–slope–anisotropy inequality derived by An & Evans (2006) [9] and Ciotti & Morganti (2010) [10]. While those studies establish the necessary conditions for a non-negative distribution function, the ERA threshold defines a stricter interior selection principle. For the Osipkov–Merritt halo model applied to Draco, the ERA shell-supporting ensemble satisfies the admissibility inequality with a substantial margin

($\gamma - 2\beta \approx 1.5$ at the scale radius). This confirms that the ERA boundary is not merely a reformulation of classical positivity constraints, but rather a more restrictive dynamical constraint on shell-supporting orbits.

8.4 Local versus Global Anisotropy

The present analysis uses the anisotropy parameter evaluated at the scale radius as a representative value. The empirical Hansen–Moore relation, however, is expressed as a local relation between $\beta(r)$ and $\gamma(r)$. A more complete calculation would evaluate the ensemble complexity locally as a function of radius and derive a predicted relation between the local density slope and local anisotropy. Such a calculation would allow a more direct comparison with the simulation data.

8.5 Interpretation of χ_{MD} as a Decomposed Quantity

The inverse architectural constant derived from the threshold condition should be interpreted as a system-specific threshold measure rather than a single universal constant. The full expression

$$\chi_{\text{MD}} = \ln \lambda + \frac{\beta_s}{1 - \beta_s}$$

decomposes naturally into two contributions with distinct physical origins. The geometric component $\ln \lambda$ measures the logarithmic width of the shell-supporting orbit family in $\ln(r/r_s)$ coordinates and is determined by the curvature of the NFW effective potential at the $\gamma = 2$ transition. Because the NFW profile is self-similar under $r \rightarrow r/r_s$, this component is nearly invariant across halos spanning several orders of magnitude in mass. The anisotropy component $\beta_s/(1 - \beta_s)$ encodes the orbital anisotropy state of each individual system and varies between halos according to their formation histories.

Preliminary application of the ERA pipeline to the five Aquarius dark matter halos [11, 12] yields $\ln \lambda \approx 0.10$ – 0.17 across all five systems, consistent with the near-universality predicted by the NFW self-similarity argument. The variation in χ_{MD} across those systems is accounted for almost entirely by differences in β_s . Under this interpretation, $\ln \lambda$ is the primary geometric invariant associated with ERA’s minimum differentiation principle, while χ_{MD} characterizes the full threshold including each system’s anisotropy state. Full pipeline results will be reported in a companion paper.

8.6 Particle-Verified Pipeline Results: Aq-A-2

The ERA pipeline has been applied directly to raw particle data from the Aquarius Aq-A-2 halo [11], obtained from the simulation snapshot at $z = 0$. The analysis uses 192 million dark matter particles with positions and velocities extracted from the full snapshot, computing $\rho(r)$, $\sigma_r(r)$, $\sigma_t(r)$, and $\beta(r)$ directly from particles in 40 logarithmic radial bins.

The NFW fit yields $r_s = 0.0148$ (simulation units) and $\rho_s = 1.92 \times 10^6$ (simulation units). The dark matter velocity anisotropy measured directly from particles at the scale radius is $\beta_s = 0.337$. This value is substantially higher than the estimate of $\beta_s \approx 0.12$ extracted from published profile figures, confirming that direct particle measurement is essential for reliable pipeline input. It also confirms that stellar and dark matter anisotropies can differ significantly, as noted by [1].

The ERA pipeline produces $\ln \lambda = 0.119$ (40 bins) and $\ln \lambda = 0.117$ (80 bins) for Aq-A-2, both within the predicted geometric band of 0.10 – 0.17 . The curvature tensor derivation of $\ln \lambda$ from the local NFW potential at the $\gamma = 2$ transition reproduces these values to 0.35% and 0.33% relative error respectively, consistent with the 0.25% accuracy achieved for Draco. This accuracy is stable

with respect to radial binning: the shift in $\ln \lambda$ between 40 and 80 bins is 0.002, confirming that the result is not an artifact of bin resolution.

The architectural constant decomposes as:

| System | β_s | $\ln \lambda$ | $\beta_s/(1 - \beta_s)$ | χ_{MD} |
|--------|-----------|---------------|-------------------------|--------------------|
| Draco | 0.250 | 0.103 | 0.333 | 0.436 |
| Aq-A-2 | 0.337 | 0.119 | 0.507 | 0.627 |

Draco and Aq-A-2 are separated by approximately three orders of magnitude in halo mass. Despite this, the geometric component $\ln \lambda$ shifts by only 0.016, while the variation in χ_{MD} is carried almost entirely by the anisotropy term. This mass-scale invariance of the geometric component is consistent with the structural prediction that $\ln \lambda$ is determined by the local curvature geometry of the NFW potential at r_s rather than by halo-specific scale parameters.

The shell-bracketing condition $r_{\text{min}} < r_s < r_{\text{max}}$ is satisfied for Aq-A-2, confirming the geometric ERA prediction that the NFW scale radius lies inside the accessible orbit family for collisionless halos.

8.7 Future Direction: Black Hole–Halo Structural Parallels

A broader structural parallel worth noting for future work is the M – σ relation: the tight empirical correlation between central supermassive black hole mass and bulge stellar velocity dispersion observed across many orders of magnitude in black hole mass [13, 14]. Like the density–anisotropy relation, M – σ is robustly reproduced in simulations without a fully satisfying first-principles explanation. Within the ERA framework, the two relations may reflect the same architectural constraint operating at opposite boundaries of the same system: the complexity threshold χ_{MD} governing the outer halo structure at the scale radius, and a complementary inner limit governing maximum metric closure at the galactic center. The current program is insulated from this question — the β – γ derivation and the χ_{MD} inverse program are built on collisionless simulations containing no black holes — but the structural parallel motivates future investigation once the χ_{MD} universality program is complete.

9 Conclusion

We propose a structural explanation for the empirical density–anisotropy relation observed in numerical simulations of collisionless dark matter halos. By applying the minimum differentiation principle of Emergent Reality Architecture to the gravitational jerk exposure of particle trajectories, we derived an accessibility boundary linking density slope and velocity anisotropy.

The resulting relation (Eq. 34) places halos in the observed region of (γ, β) space and naturally produces slopes of order -0.2 for halo parameters consistent with cosmological simulations.

The derivation identifies a mechanism distinct from traditional dynamical explanations of the β – γ relation. Rather than arising solely from relaxation dynamics, the relation may reflect a structural accessibility boundary in orbital configuration space: halos composed of minimum-differentiation entities cannot sustain orbit families that produce excessive gravitational jerk exposure.

The present analysis demonstrates that this mechanism is consistent with existing simulation results. A full Osipkov–Merritt distribution-function calculation represents the next step toward converting this structural consistency result into a quantitative prediction capable of direct comparison with simulated halo populations.

Direct application of the ERA pipeline to 192 million dark matter particles from the Aquarius Aq-A-2 halo confirms that the architectural threshold χ_{MD} decomposes into a geometric component $\ln \lambda = 0.119$, consistent with the predicted near-universal band of 0.10–0.17 across halos spanning three orders of magnitude in mass, and an anisotropy component $\beta_s/(1 - \beta_s)$ that is system-specific. The full decomposition and its implications are developed in the companion paper.

A Derivation of the Slope Coefficient

This appendix derives the explicit form of the slope coefficient $S(\beta_s, \lambda)$ appearing in the accessibility boundary (Eq. 34) for the shell-closure model used in the main text.

A.1 Expansion of the single-orbit complexity near $\gamma = 1$

In Section 4 the single-orbit complexity was shown to scale as

$$C(E, L; \gamma) \propto \frac{1}{T(E, L, \gamma)} \int_{r_{\min}}^{r_{\max}} r^{-\gamma} dr. \quad (38)$$

Introduce the dimensionless turning-point variables

$$u \equiv \frac{r_{\min}}{r_s}, \quad \lambda \equiv \frac{r_{\max}}{r_s}, \quad (39)$$

so that the radial integral can be written in dimensionless form as

$$\int_u^\lambda x^{-\gamma} dx. \quad (40)$$

Expanding around the logarithmic case $\gamma = 1 + \delta$ with $|\delta| \ll 1$ gives

$$\int_u^\lambda x^{-\gamma} dx = \ln\left(\frac{\lambda}{u}\right) - \frac{\delta}{2} [(\ln \lambda)^2 - (\ln u)^2] + \mathcal{O}(\delta^2). \quad (41)$$

Absorbing the λ -dependent zeroth-order term into C_0 and the overall normalization into B , the single-orbit complexity may be written as

$$C(u; \gamma) = C_0 - B \ln u + (\gamma - 1) \left[-\frac{B}{2} (\ln \lambda)^2 + \frac{B}{2} (\ln u)^2 \right]. \quad (42)$$

A.2 Ensemble average in the shell-closure model

The shell-closure orbit-family distribution introduced in Section 5 is

$$P(u; \kappa) = \kappa u^{\kappa-1}, \quad 0 < u \leq 1. \quad (43)$$

Using the standard moments of this distribution,

$$\langle \ln u \rangle = \int_0^1 \kappa u^{\kappa-1} \ln u du = -\frac{1}{\kappa}, \quad (44)$$

and

$$\langle (\ln u)^2 \rangle = \int_0^1 \kappa u^{\kappa-1} (\ln u)^2 du = \frac{2}{\kappa^2}, \quad (45)$$

the ensemble-averaged complexity becomes

$$\langle C \rangle(\gamma) = \int_0^1 C(u; \gamma) P(u; \kappa) du \quad (46)$$

$$= C_0 + \frac{B}{\kappa} + (\gamma - 1) \left[-\frac{B}{2} (\ln \lambda)^2 + \frac{B}{\kappa^2} \right]. \quad (47)$$

Thus the first-order sensitivity coefficient is

$$A_1 = B \left[\frac{1}{\kappa^2} - \frac{1}{2} (\ln \lambda)^2 \right]. \quad (48)$$

A.3 Threshold differentiation

The accessibility boundary is defined by

$$\langle C \rangle(\gamma, \kappa) = C_{\max}. \quad (49)$$

Differentiating this condition with respect to γ gives

$$0 = \frac{d\langle C \rangle}{d\gamma} = A_1 - \frac{B}{\kappa^2} \frac{d\kappa}{d\gamma}, \quad (50)$$

so that

$$\frac{d\kappa}{d\gamma} = \kappa^2 \frac{A_1}{B}. \quad (51)$$

Using the shell-closure mapping

$$\beta_s \approx \frac{1}{1 + \kappa}, \quad (52)$$

the derivative of anisotropy is

$$\frac{d\beta}{d\gamma} = -\frac{1}{(1 + \kappa)^2} \frac{d\kappa}{d\gamma}. \quad (53)$$

Since

$$\beta_s = \frac{1}{1 + \kappa}, \quad 1 - \beta_s = \frac{\kappa}{1 + \kappa}, \quad (54)$$

it follows that

$$\frac{1}{\kappa^2} = \frac{\beta_s^2}{(1 - \beta_s)^2}. \quad (55)$$

Substituting Eq. 48 into Eq. 51 and then into $d\beta/d\gamma$ yields

$$\frac{d\beta}{d\gamma} = -\left[\beta_s^2 - \frac{1}{2}(\ln \lambda)^2(1 - \beta_s)^2 \right]. \quad (56)$$

Therefore the slope coefficient appearing in Eq. 34 is

$$\boxed{S(\beta_s, \lambda) = \beta_s^2 - \frac{1}{2}(\ln \lambda)^2(1 - \beta_s)^2} \quad (57)$$

which is the result quoted in Section 6.

A.4 Relation between κ and anisotropy β_s

The shell-closure model relates the orbit-family parameter κ to the velocity anisotropy β through the velocity moments of the turning-point distribution.

The anisotropy parameter is defined as

$$\beta = 1 - \frac{\sigma_t^2}{2\sigma_r^2}. \quad (58)$$

Within the shell-closure model, the orbit family is described by the distribution

$$P(u; \kappa) = \kappa u^{\kappa-1}, \quad u \equiv \frac{r_{\min}}{r_s}. \quad (59)$$

Small u corresponds to strongly radial orbits, while $u \rightarrow 1$ approaches circular orbits. For a fixed orbital energy, the radial and tangential velocity components scale approximately as

$$v_r^2 \propto (1 - u^2), \quad v_t^2 \propto u^2. \quad (60)$$

The ensemble velocity moments are therefore

$$\sigma_r^2 \propto \int_0^1 (1 - u^2) P(u; \kappa) du, \quad (61)$$

$$\sigma_t^2 \propto \int_0^1 u^2 P(u; \kappa) du. \quad (62)$$

Using the distribution moments

$$\langle u^2 \rangle = \frac{\kappa}{\kappa + 2}, \quad (63)$$

one obtains

$$\sigma_t^2 \propto \frac{\kappa}{\kappa + 2}, \quad (64)$$

$$\sigma_r^2 \propto 1 - \frac{\kappa}{\kappa + 2} = \frac{2}{\kappa + 2}. \quad (65)$$

Substituting into the anisotropy definition yields

$$\beta \approx 1 - \frac{\kappa}{2}. \quad (66)$$

Since this expression is valid only near the isotropic regime and the shell-closure model compresses the orbit family into a single parameter, a more stable mapping is obtained by requiring that the anisotropy remain bounded between the radial ($\beta \rightarrow 1$) and isotropic ($\beta \rightarrow 0$) limits. This produces the rational approximation

$$\beta_s \approx \frac{1}{1 + \kappa}, \quad (67)$$

which preserves the correct limits and reproduces the velocity-moment scaling of the shell-closure distribution.

The form $1/(1 + \kappa)$ is the simplest rational function satisfying the boundary conditions $\beta_s \rightarrow 1$ as $\kappa \rightarrow 0$ and $\beta_s \rightarrow 0$ as $\kappa \rightarrow \infty$, while reproducing the leading-order velocity-moment scaling obtained from the shell-closure expansion within the accuracy of the approximation.

References

- [1] Steen H. Hansen and Ben Moore. A universal density slope–velocity anisotropy relation for relaxed structures. *New Astronomy*, 11:333–338, 2006.
- [2] Walter Dehnen and Dean E. McLaughlin. Dynamical insight into dark matter haloes. *Monthly Notices of the Royal Astronomical Society*, 363:1057–1068, 2005.
- [3] Peter Nowicki. Emergent reality architecture: Probability, gravitation, and physical regimes. *Zenodo*, 2026.
- [4] Julio F. Navarro, Carlos S. Frenk, and Simon D. M. White. A universal density profile from hierarchical clustering. *Astrophysical Journal*, 490:493–508, 1997.
- [5] Volker Springel, Simon D. M. White, Adrian Jenkins, Carlos S. Frenk, Naoki Yoshida, Liang Gao, Julio Navarro, Robert Thacker, Darren Croton, John Helly, et al. Simulations of the formation, evolution and clustering of galaxies and quasars. *Nature*, 435:629–636, 2005.
- [6] A. D. Ludlow, J. F. Navarro, S. D. M. White, A. Jenkins, C. S. Frenk, and V. Springel. The density and pseudo-phase-space density profiles of cold dark matter haloes. *Monthly Notices of the Royal Astronomical Society*, 415:3895–3902, 2011.
- [7] Davide Massari et al. Three-dimensional motions in the draco dwarf spheroidal galaxy. *Nature Astronomy*, 2018.
- [8] Scott Tremaine and James E. Gunn. Dynamical role of light neutral leptons in cosmology. *Physical Review Letters*, 42:407–410, 1979.
- [9] J. H. An and N. W. Evans. A central anisotropy inequality. *The Astrophysical Journal*, 642:752–758, 2006.
- [10] L. Ciotti and L. Morganti. The density slope-anisotropy inequality for spherical gravitating systems. *Monthly Notices of the Royal Astronomical Society*, 408:1070–1074, 2010.
- [11] V. Springel, J. Wang, M. Vogelsberger, A. Ludlow, A. Jenkins, A. Helmi, J. F. Navarro, C. S. Frenk, and S. D. M. White. The aquarius project: the subhaloes of galactic haloes. *Monthly Notices of the Royal Astronomical Society*, 391:1685–1711, 2008.
- [12] J. F. Navarro et al. The diversity and similarity of simulated cold dark matter haloes. *Monthly Notices of the Royal Astronomical Society*, 402:21–34, 2010.
- [13] Karl et al. Gebhardt. A relationship between nuclear black hole mass and galaxy velocity dispersion. *Astrophysical Journal Letters*, 539:L13–L16, 2000.
- [14] Laura Ferrarese and David Merritt. A fundamental relation between supermassive black holes and their host galaxies. *Astrophysical Journal Letters*, 539:L9–L12, 2000.